Elastic Distortions of Carbon Nanotubes Induced by Chiral Fullerene Chains.

Jamie H. Warner*,[1] and Mark Wilson[2]

[1]Department of Materials, University of Oxford, Parks Rd, Oxford, OX1 3PH, United Kingdom. and [2]Department of Chemistry, Physical and Theoretical Chemistry Laboratory, University of Oxford, South Parks Rd, Oxford, OX1 3QZ, United Kingdom

ARTICLE

ABSTRACT We show that when $Y@C_{82}$ metallofullerenes are inserted into single-walled carbon nanotubes (SWNTs) with large diameters of 2 nm, the minimum energy configuration is a double-helix chiral structure extending over hundreds of nanometers. We demonstrate rotation of the double-helix fullerene chain within the nanotube host that induces real time elastic distortions of the nanotube in a crank-shaft manner. Molecular dynamics simulations, employing an atomic description of the confining SWNT and a reduced description of $Y@C_{82}$, reproduce the key experimental observations.

KEYWORDS: Peapods · fullerenes · SWNTs · chirality · HRTEM

INTRODUCTION

For more than 400 years scientists have studied sphere packing arrangements in volumetric spaces.[1,2] The insertion of spherical fullerenes into cylindrical carbon nanotubes leads to the formation of carbon nanopeapods.[3] Gravitational forces are minimal and it is the competition between surface forces and mechanical structure that define the lowest energy arrangements.[4−7] There is no covalent bonding between the fullerenes and nanotube in a nanopeapod and the minimum energy configuration is influenced by the strong van der Waals forces between the fullerenes and single-walled carbon nanotubes (SWNTs). In graphite, the van der Waals separation between the stacked graphene layers is 0.34 nm. This distance typifies sp^2 carbon graphitic layers where interactions between the π orbitals are present. In order to achieve uniform 1D packing of fullerenes inside SWNTs, the separation between the fullerene and SWNT should also be on the order of the graphitic van der Waals separation. Since the diameter of fullerenes ranges between ~0.7 nm (C_{60}) to ~0.85 nm (C_{82}), the diameter range of nanotubes needs to be between 1.4 − 1.6 nm, if they are to pack tightly to form a 1D chain.[8] This route enables the formation of 1D spin chain systems by inserting paramagnetic endohedral fullerenes such as $Sc@C_{82}$, $Y@C_{82}$ and $La@C_{82}$, which are of interest for spintronics and quantum information processing applications.[9] However, when the diameter of the SWNT increases beyond 1.6 nm it is not possible for the fullerene to be located at the center of a cylindrical SWNT and still be at the graphitic van der Waals distance of 0.34 nm from the sidewalls. This means that the structure of the composite system is likely to change in the form of different packing structures (i.e 2D zigzag) and/or distortion of the atomic structure of the SWNT or fullerenes. The insertion of C_{60} into nanotubes with larger diameters has been shown to result in different packing phases.[6,10,11]

At the simplest level one might expect the packing problem to map onto the phase diagram for hard spheres confined into cylinders.[12] However, carbon nanotubes have one of the highest elastic modulus of all known materials.[13] The strong attractive van der Waals forces between carbon nanotubes lead to their tight bundling and adhesion to surfaces.[14,15] When the diameter of SWNTs reaches above 2 nm the cross-sectional shape of the nanotubes can change.[14] Large diameter nanotubes become distorted when placed on surfaces in order to maximize the contact area involving the surface forces[14] and when they bundle together it can also lead to similar distortions.[15] The diameter of a SWNT can become large enough that the attractive forces between its walls lead to its collapse and the loss of the free space in the interior.[16,17] The implication is that mapping onto a rigid sphere/cylinder system may be too simplistic.

*Jamie.warner@materials.ox.ac.uk.

Received for review May 20, 2010 and accepted June 25, 2010.

Published online July 12, 2010.
10.1021/nn101111b

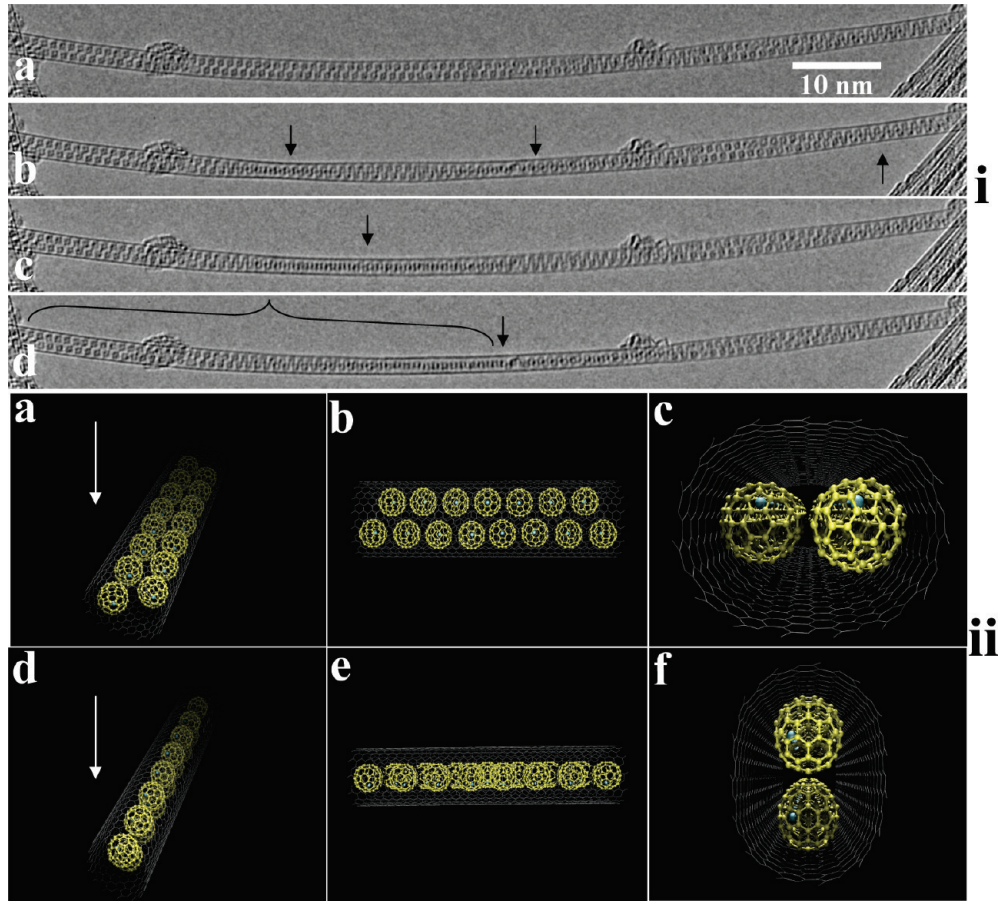

Figure 1. (i) Time-series (a) - (d) of HRTEM images showing a suspended carbon nanotube peapod containing Y@C_{82} fullerenes with double-helix chiral packing. Time between frames is 5 s. (ii) Atomic representation of the trigonal packing of Y@C_{82} metallofullerenes in elliptically distorted (15,13) SWNT with (a) 3D perspective with major axis of SWNT perpendicular to HRTEM viewing direction, indicated by arrow. (b) Top view of (a). (c) End view of (a). (d) 3D perspective with major axis of SWNT parallel to HRTEM viewing direction, indicated by arrow. (e) Top view of (d). (f) End view of (d).

Evidence for structural changes of carbon nanotubes when they are filled with material has been limited.[18,19] This is due to the relatively small diameters of the SWNTs used for filling (<1.6 nm), or the relatively small areas studied, or the use of multiwalled carbon nanotubes that are less susceptible to structural distortions. In some cases, slight perturbation to the cross-sectional profile of the nanotubes occurs when filled with materials such as cobalt iodide.[18]

To date there has been no investigation of the 2D packing phases of metallofullerenes in carbon nanopeapods. Although a large number of metallofullerenes have been inserted into carbon nanotubes the question arises as to whether they can adopt 2D packing like C_{60}. Metallofullerenes typically have charged cages (i.e $La^{3+}@C_{82}^{3-}$) compared to C_{60} and this may influence the surface forces that govern the resulting structure formed in the composite nanomaterial. The formation of complex packing configurations of paramagnetic metallofullerenes may lead to new behavior in the spin dynamics and the transfer of spin information along the chain length.[20]

RESULTS AND DISCUSSION

In order to investigate the intrinsic packing structure of paramagnetic metallofullerenes we used SWNTs with diameters up to 2.4 nm and Y@C_{82} for peapod fabrication. An important component of our work was to take extra care to debundle the peapods by sonication in 1,2-dichloroethane and evaporating the solvent rapidly when preparing TEM samples. This ensured long isolated peapods were suspended in free space on a lacey grid for analysis and eliminates any intertube forces present in bundles that may lead to distortions. Peapods with nanotube diameters between 1.35−1.7 nm showed typical 1D packing of fullerenes as previously reported.[8,9] However, we found that peapods formed in nanotubes with a diameter of ~2 nm exhibit unique packing of the Y@C_{82} that has, to our knowledge, never been previously observed for metallofullerenes. The packing is of trigonal form with a chiral twist, resulting in double-helix structures. We found that the diameter of the nanotube was distorted along its length by the double-helix packing configuration of the Y@C_{82}.

Figure 1(i)(a) shows a typical isolated peapod over 100 nm in length suspended over free space. This long isolated suspended structure enables the intrinsic structural configuration of the peapod to be examined. The use of 1,2-dicholoroethane was important to achieve this as it enables debundling of the peapods without using a surfactant, such as sodium dodecyl sulfate (SDS), that attaches to the surface of the peapod and prevents high quality images to be obtained of the fullerenes inside. Surfactants wrapped around peapods may also restrict the ability of the SWNT to distort. 2D trigonal packing of the $Y@C_{82}$ is seen with a slight rotational twist observed toward the right-hand side.

Figure 1(i)(b) shows the $Y@C_{82}$ peapod after 5 s of electron beam irradiation and significant differences in the packing structure are apparent. Three regions of crossover in the double-helix chiral twist are seen and indicated by arrows. These crossover regions also show a reduction in the apparent nanotube diameter. This is due to the distortion of the carbon nanotube cross section by the 2D fullerene packing. The nanotube conforms to an elliptical shape that matches the trigonal packing of the $Y@C_{82}$ and as the 2D fullerene chain twists, so too does the projection of the elliptical cross-section of the nanotubes. Figures 1(i)(c) and 1(i)(d) are taken in 5 s intervals after figure 1(i)(b) and show the double-helix $Y@C_{82}$ packing rotates under electron beam irradiation and induces elastic modifications to the nanotube cross-sectional shape. The length scale of the pitch of the twist in the fullerene chain is up to 50 nm in figure 1(i)(d), indicated by the bracket. This is extraordinarily long compared to the 5 nm length scale of pitch previously observed for C_{60} helical packing.[6]

Line profiles that plot the gray scale intensity as a function of distance were taken perpendicular to the nanotubes axis. We measured the shortest cross-sectional diameter to be 1.67 nm and the longest to be 2.21 nm, giving rise to a difference of 0.54 nm between the two and corresponding to an eccentricity, $\epsilon = 0.65$. If we take the average of these two values to be equal to the unperturbed diameter of the nanotubes if it was not filled we get 1.94 nm. We measured the chiral angle of the nanotubes by directly imaging the atomic structure and performing a 2D FFT. Combining the chiral angle and a diameter of 1.94 nm we index the nanotube in figure 1 as (n,m) = (15, 13), which is semiconducting. Figure 1(ii) shows an atomic structural model of the trigonal packing of the $Y@C_{82}$ in a (15, 13) SWNT with an induced elliptical distortion on the same scale as observed in HRTEM analysis. Figures 1(ii)(a) - 1(ii)(c) show three different perspectives (3D, top view, and end view) when the major axis is orientated perpendicular to the HRTEM viewing direction. In figures 1(ii)(d) - 1(ii)(f) the major axis is orientated parallel to the HRTEM viewing direction. This illustrates the difference in HRTEM projection for the two different orientations of the $Y@C_{82}$ packing and the concomitant change in the diameter of the SWNT host.

The packing structure of the $Y@C_{82}$ in the SWNT can be examined in detail when the major axis is perpendicular to the HRTEM viewing direction. Figures 2(i)(a) and 2(i)(c) examine the trigonal packing structure in detail and figures 2(i)(b) and 2(i)(d) the occasionally observed square packing configuration. The density of fullerene packing is greater for trigonal packing compared to the square packing. The average inter-$Y@C_{82}$ distance is also larger for the square packing compared to trigonal packing. The diameter of the SWNT host for the square packing is also larger than the diameter for trigonal packing. This highlights the link between fullerene crystallization and nanotube diameter.

Figure 2(ii) shows the time-dependent HRTEM images of the 2D packing of $Y@C_{82}$ in a peapod with 10 s between frames. In figure 2(ii)(a) a defect in the crystal lattice is seen, indicated by an arrow. Red shade is used in figure 2(ii) to highlight holes within the crystal lattice formed by the presence of defects. In figure 2(ii)(b) the defect has been removed by adjustment of the position of fullerenes. In figure 2(ii)(c) a large hole is formed, indicated by the red region and 10 s later, figure 2(ii)(d), a large group of seven $Y@C_{82}$ fullerenes have propagated to the left, resulting in the movement of the hole to a new position. In figure 2(ii)(e), reconfiguration of the $Y@C_{82}$ leads to the hole being located primarily in the bottom region. In figure 2(ii)(f) the hole has moved toward the left and in figure 2(ii)(g) it has separated into two smaller regions. Figure 2(ii)(g) shows that the chain has twisted with concomitant change in SWNT diameter, but the positioning of the holes remains the same. This illustrates the freedom of $Y@C_{82}$ fullerenes to move about within the 2D crystal structure and to adjust their position. The presence of a small defect or hole does not lead to the degradation of the packing.

To further rationalize the experimental observations, molecular dynamics (MD) simulations are performed using highly simplified descriptions of the interatomic interactions. The carbon nanotubes are modeled atomistically using a Tersoff-II potential.[21] In order to greatly simplify the problem, the $Y@C_{82}$ units are mapped onto sphere of diameter 10.2 Å and their interactions with each other and with the carbon atoms comprising the SWNT are modeled with Lennard-Jones (LJ) potentials. As a result, the problem has been effectively reduced to one of sphere packing within a flexible cylinder.

In order to probe the underlying energy landscape, energy minimization calculations are performed in which the positions of both the LJ spheres and the carbon atoms comprising the SWNT are allowed to evolve in time and in which the number of LJ spheres inside the SWNT is varied (effectively controlling the number

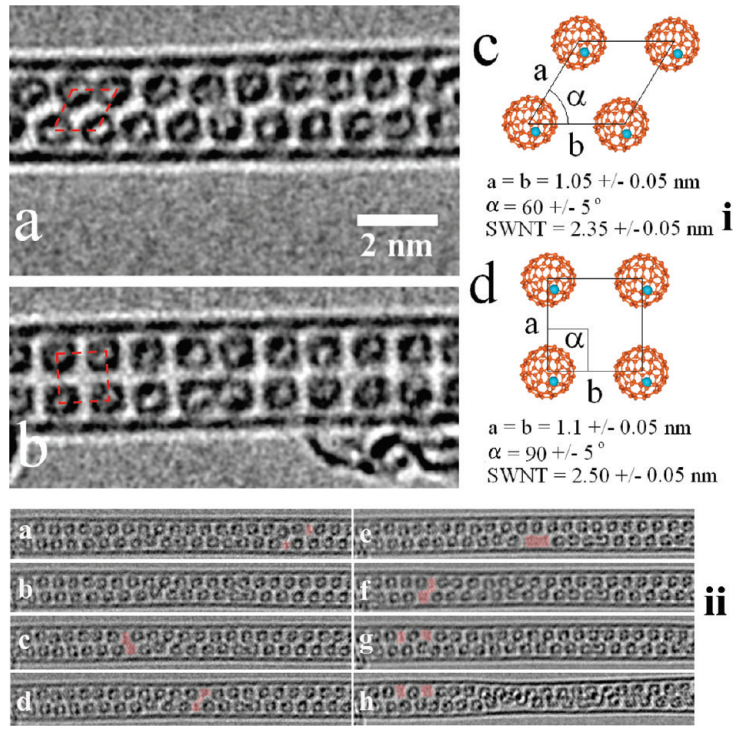

Figure 2. (i) HRTEM images of (a) close-packed Y@C_{82} and (b) square-packed Y@C_{82}. (c) Schematic of Y@C_{82} observed in HRTEM images with trigonal packing. (d) Schematic of Y@C_{82} observed in HRTEM images with square packing. (ii) Time-series of HRTEM images showing the movement of lattice defect in the Y@C_{82} packing (i.e hole). Shaded red-areas indicate newly formed holes.

density per unit length along the SWNT major axis). Local energy minima are located at a range of particle densities corresponding to the stability fields of different packing environments (as observed, for example, for the packing of hard spheres into incompressible cylinders[12]). Figures 3(i) and 3(ii) show a molecular graphics "snapshot" of a structure for one such local minima corresponding to a pseudoclose-packed trigonal lattice arrangement, shown both looking along the SWNT major axis (figure 3(ii)) and perpendicular to this (figure 3(i)), highlighting the significant eccentricity ($\epsilon = 0.68$) inherent in the structure of the energy-minimized SWNT. This computed eccentricity is similar to the value ($\epsilon = 0.65$) determined from HRTEM images in figure 1.

Molecular dynamics simulations are performed over a range of temperatures at densities corresponding to

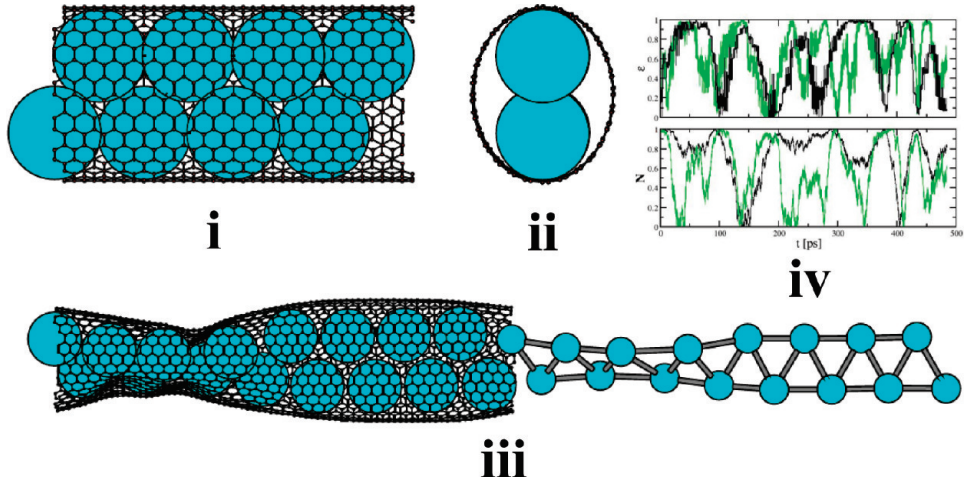

Figure 3. Molecular graphics "snapshot" of an energy minimized trigonal lattice structure formed from the LJ spheres encased in a (15, 15) SWNT viewed (i) perpendicular to the major axis and (ii) along the major axis. (iii) Molecular graphics "snapshot" of a trigonal LJ lattice evolving dynamically at $T = 400$K, highlighting the high correlation between the SWNT eccentricity and the trigonal lattice orientation. The right-hand section shows the LJ lattice with the encasing SWNT cut away to highlight the inherent rotational distortion along the major axis. (iv) The projection of the eccentricity and normal vectors (upper and lower panels respectively) at $T = 400$ K (black lines) and $T = 600$ K (green lines) for a specified section of the SWNT and a single trigonal lattice unit. The figures highlight both the significant rotations observed on the simulation timescales and the high correlation between these two vectors.

the local energy minima. Figure 3(iii) shows a "snapshot" from a simulation run at 400 K. The integrity of the trigonal lattice structure is retained over the simulation time-scale with an associated rotation of the lattice about the SWNT major axis. In order to quantify the nature of this rotational motion two vector quantities are monitored as a function of time. First, a vector N is defined as normal to the plane containing three spheres comprising a single trigonal unit. Second, the SWNT is divided into 10 sections along the major axis and a vector ϵ is defined for each section pointing from the center of mass of that section along the major eccentric axis and confined to a plane perpendicular to the SWNT major axis. Figure 3(iv) shows the time evolution of these two vectors projected along a single Cartesian axis exemplified for a single trigonal unit confined within a given SWNT section. Both the SWNT eccentricity and trigonal lattice vectors are observed to rotate over the simulation time-scale. As might be anticipated for a simple activated process, the time-scales of these rotations appear to decrease with increasing temperature. In addition, there appears a clear correlation between these two vectors. Indeed, the distribution of the dot product N.ϵ calculated time-averaged using all of the trigonal units and over the whole length of the SWNT shows a clear peak at zero, indicating that these vectors are highly correlated normal to one another, highlighting the strong correlation between the rotation of the trigonal units and the eccentricity of the confining SWNT. This suggests that the observations in the HRTEM are due to the rotation of the 2D trigonal fullerene crystal within the SWNT leading to its distortion rather than the rotation of the entire structure with respect to the viewing projection.

CONCLUSION

In nature, chirality in biomolecular structure is readily found, such as in DNA. Our experimental results show that chiral twists are present in the ground state configuration of nanoscale systems such as in carbon nanopeapods. The chirality of fullerene crystallization is concomitant with the elliptical distortion of the nanotubes and is generated by combining spherical fullerenes with cylindrical nanotubes. It is the nanoscopic surface interactions between these nanomaterials that lead to the complex 3D geometries. Our molecular dynamics simulations suggest that the time-dependent changes to the diameter of the nanopeapod captured with HRTEM is due to the chain of fullerenes rotating within the nanotubes accompanied by a localized elastic distortion to the nanotubes cross section and not a rotation of the entire nanopeapod structure. Allowing some inherent flexibility in the nanotube's structure, results in trigonal packing with elliptical SWNT cross-section. Since there is no covalent bonding between the fullerenes and nanotubes, the chiral chain of fullerenes is free to rotate within the nanotube. By supplying energy to the system, a chiral chain of fullerenes can drive elastic distortions to the perpendicular axis of a nanotube in a crank-shaft manner.

METHODS SUMMARY

FH-P-type single-walled carbon nanotubes were generously provided by Meijo nanocarbon. The SWNTs were treated to high temperature annealing under dynamic vacuum to remove catalyst particles and amorphous carbon. Y@C_{82} metallofullerenes were produced using a custom-built arc-discharge system and purified using HPLC. Peapods were formed by dropping a solution of Y@C_{82} in CS_2 onto buckypaper and allowing to dry. The composite was placed in a quartz tube, sealed under vacuum and heated for 4 days at 470 °C to form peapods. The peapods were dispersed in 1,2-dichloroethane using sonication for 30 min. A drop of the peapod solution was deposited onto a lacey carbon coated TEM grid sitting on filter paper and allowing to dry. This ensured that the peapods were debundled and dispersed on the TEM grid. HRTEM was performed using Oxford's JEOL JEM-2200MCO field-emission transmission electron microscope, fitted with probe and image aberration correctors and operated at an accelerating voltage of 80 kV. Data was recorded using a Gatan Ultrascan 4k × 4k CCD camera.

The carbon nanotube is modeled using a Tersoff-II potential[21] which reproduces key structural and dynamic properties.[22] The Y@C_{82} units are mapped onto spheres of diameter 10.2 Å and their interactions with each other and with the carbon atoms comprising the carbon nanotube are modeled using Lennard-Jones potentials, requiring the specification of four parameters, the sphere−sphere and sphere-carbon well depths, $\epsilon_{\alpha\beta}$, ($\alpha\beta$=Sp,C), and the diameters $\sigma_{\alpha\beta}$. The sphere−sphere interactions are parametrized by reference to the approximate diameter of Y@C_{82} (σ_{SpSp}. = 10.2 Å) and by reference to a previous fullerene potential which gives a useful approximate well depth, ϵ_{SpSp}/k_B = 3260 K. The carbon-sphere interactions are parametrized using standard mixing rules combined with an existing carbon Lennard-Jones potential,[23] giving $\sigma_{SpC} = (1/2)(\sigma_{SpSp}+\sigma_{CC})$ and $\epsilon_{SpC}^2 = \epsilon_{SpSp}\epsilon_{CC}$, where σ_{CC} = 3.40 Å and ϵ_{CC}/k_B = 28 K respectively. Molecular dynamics and energy minimization calculations are performed on systems containing between 1200 and 4800 carbon atoms (corresponding to between 20 and 80 unit cells of a (15, 15) SWNT) and between 8 and 32 LJ spheres. A (15, 15) SWNT is chosen because it has a diameter close to that observed experimentally coupled with a relatively short unit cell repeat length. The molecular dynamics calculations are performed in the NVT ensemble at temperatures between 200 and 1000 K. The initial velocities are sampled from a Gaussian distribution and the temperature is maintained using Nosé-Hoover thermostats.[24,25]

Acknowledgment. We thank Meijo Nano-Carbon for the generous supply of high-purity SWNTs. JHW thanks the support from the Violette and Samuel Glasstone Fund and Brasenose College, University of Oxford. We thank N. Young and A. Kirkland for assistance with electron microscopy and Y. Ito, K. Porfyrakis and A. Briggs for assistance with fullerenes.

REFERENCES AND NOTES

1. Sloane, N. J. A. Kepler's Conjecture Confirmed. *Nature* **1998**, *395*, 435.
2. Hales, T. C. Sphere Packings, I. *Discrete Comput. Geom.* **1997**, *17*, 1–51.
3. Smith, B. W.; Monthioux, M.; Luzzi, D. E. Encapsulated C_{60} in Carbon Nanotubes. *Nature* **1998**, *396*, 323–324.
4. Troche, K. S.; Coluci, V. R.; Braga, S. F.; Chinellato, D. D.;

Sato, F.; Legoas, S. B.; Rurali, R.; Galvao, D. S. Prediction of Ordered Phases of Encapsulated C_{60}, C_{70} and C_{78} Inside Carbon Nanotubes. *Nano Lett.* **2005**, *5*, 349–355.
5. Yoon, M.; Berber, S.; Tomanek, D. Energetics and Packing of Fullerenes in Nanotubes Peapods. *Phys. Rev. B.* **2005**, *71*, 155406.
6. Khlobystov, A. N.; Britz, D. A.; Ardavan, A.; Briggs, G. A. D. Observation of Ordered Phases of Fullerenes in Carbon Nanotubes. *Phys. Rev. Lett.* **2004**, *92*, 245507.
7. Hodak, M.; Girafalco, L. A. Ordered Phases of Fullerene Molecules Formed Inside Carbon Nanotubes. *Phys. Rev. B.* **2003**, *67*, 075419.
8. Hirahara, K.; Suenaga, K.; Bandow, S.; Kato, H.; Okazaki, T.; Shinohara, H.; Iijima, S. One-Dimensional Metallofullerenes Crystal Generated Inside Single-Walled Carbon Nanotubes. *Phys. Rev. Lett.* **2000**, *85*, 5384–5387.
9. Warner, J. H.; Watt, A. A. R.; Ge, L.; Porfyrakis, K.; Akachi, T.; Okimoto, H.; Ito, Y.; Ardavan, A.; Montanari, B.; Jefferson; et al. Dynamics of Paramagnetic Metallofullerenes in Carbon Nanotube Peapods. *Nano Lett.* **2008**, *8*, 1005–1010.
10. Yamazaki, T.; Kuramochi, K.; Takagi, D.; Homma, Y.; Nishimura, F.; Hori, N.; Watanabe, K.; Suzuki, S.; Kobayashi, Y. Ordered Fullerene Nanocylinders in Large-Diameter Carbon Nanotubes. *Nanotechnology* **2008**, *19*, 045702.
11. Ning, G.; Kishi, N.; Okimoto, H.; Shiraishi, M.; Sugai, T.; Shinohara, H. Structural Stability and Transformation of Aligned C_{60} and C_{70} Fullerenes in Double-Wall and Triple-Wall Carbon Nanotube Peapods. *J. Phys. Chem. C.* **2007**, *111*, 14652–14657.
12. Pickett, G. T.; Gross, M.; Okuyama, H. Spontaneous Chirality in Simple Systems. *Phys. Rev. Lett.* **2000**, *85*, 3652–3655.
13. Salvetat, J.-P.; Briggs, G. A. D.; Bonard, J.-M.; Bacsa, R. R.; Kulik, A. J.; Stockli, T.; Burnham, N. A.; Forro, L. Elastic and Shear Moduli of Single-Walled Carbon Nanotube Ropes. *Phys. Rev. Lett.* **1999**, *82*, 944–947.
14. Hertel, T.; Walkup, R. E.; Avouris, P. Deformation of Carbon Nanotubes by Surface van der Waals Forces. *Phys. Rev. B.* **1998**, *58*, 13870–13873.
15. Ruoff, R. S.; Tersoff, J.; Lorents, D. C.; Subramoney, S.; Chan, B. Radial Deformation of Carbon Nanotubes by van der Waals Forces. *Nature,* **1993**, *364*, 514–516.
16. Chopra, N. G.; Benedict, L. X.; Crespi, V. H.; Cohen, M. L.; Louie, S. G.; Zettl, A. Fully Collapsed Carbon Nanotubes. *Nature,* **1995**, *377*, 135–138.
17. Motta, M.; Moisala, A.; Kinloch, I. A.; Windle, A. H. High Performance Fibres From Dog Bone Carbon Nanotubes. *Adv. Mater.* **2007**, *19*, 3721–3726.
18. Philp, E.; Sloan, J.; Kirkland, A. I.; Meyer, R. R.; Friedrichs, S.; Hutchison, J. L.; Green, M. L. H. An Encapsulated Helical One-Dimensional Cobalt Iodide Nanostructure. *Nature Mater.* **2003**, *2*, 788–791.
19. Warner, J. H.; Ito, Y.; Zaka, M.; Ge, L.; Akachi, T.; Okimoto, H.; Porfyrakis, K.; Watt, A. A. R.; Shinohara, H.; Briggs, G. A. D. Rotating Fullerene Chains Inside Carbon Nanotubes. *Nano Lett.* **2008**, *8*, 2328–2335.
20. Bose, S. Quantum Communication Through an Unmodulated Spin Chain. *Phys. Rev. Lett.* **2003**, *91*, 207901.
21. Tersoff, J. New Empirical Approach for the Structure and Energy of Covalent Systems. *Phys. Rev. B. 37* **1988**, 6991–7000.
22. Bishop, C. L.; Wilson, M. The Filling of Flexible Carbon Nanotubes by Molten Salts. *J. Mat. Chem.* **2009**, *19*, 2929–2939.
23. Steele, W. A. Interaction of Rare-gas Atoms with Graphitized Carbon-Black. *J. Phys. Chem.* **1978**, *82*, 817–821.
24. Nosé, S. A Unified Formulation of the Constant Temperature Molecular Dynamic Methods. *J. Chem. Phys.* **1984**, *81*, 511–519.
25. Hoover, W. G. Canonical Dynamics - Equilibrium Phase-Space Distributions. *Phys. Rev. A* **1985**, *31*, 1695–1697.